Preprint Title	Flexible freestanding MoS$_2$ based paper-like material for energy conversion and storage
Authors	Florian Zoller, Jan Luxa, Thomas Bein, Dina Fattakhova-Rohlfing, Daniel Bousa and Zdenek Sofer
Article Type	Full Research Paper
Supporting Information File 1	SI File.docx; 576.3 KB
ORCID® iDs	Zdenek Sofer - https://orcid.org/0000-0002-1391-4448

Flexible freestanding MoS₂ based paper-like material for energy conversion and storage

Florian Zoller[1,2], Jan Luxa[3], Thomas Bein[1], Dina Fattakhova-Rohlfing[2,4], Daniel Bouša[3] and Zdeněk Sofer[*3]

Address:

[1]Department of Chemistry and Center for NanoScience (CeNS), Ludwig-Maximilians-Universität München (LMU Munich)

[2]Faculty of Engineering and Center for Nanointegration Duisburg-Essen (CENIDE), University of Duisburg-Essen, Lotharstraße 1, 47057 Duisburg, Germany

[3]Department of Inorganic Chemistry, University of Chemistry and Technology Prague, Technická 5, 166 28 Prague 6, Czech Republic

[4]Forschungszentrum Jülich GmbH, Institute of Energy and Climate Research (IEK-1) Materials Synthesis and Processing, Wilhelm-Johnen-Straße, 52425 Jülich, Germany

Email: zdenek.sofer@vscht.cz

* Corresponding author

Abstract

Construction of flexible electrochemical devices for energy storage and generation is of utmost importance in the modern society. In this article, we report the synthesis of flexible MoS₂ based composite paper by high-energy shear force milling and simple vacuum filtration. This composite material combines high flexibility, mechanical strength and good chemical stability. Chronopotentiometric charge-discharge

measurements were used to determine the capacitance of our paper material. Highest capacitance of 33 mF cm^{-2} was achieved at current density of 1 mA cm^{-2} showing potential application in supercapacitors. We further used the material as a cathode for hydrogen evolution reaction (HER) with an onset potential of ca. -0.2 V *vs* RHE. The onset potential was even lower (*ca.* -0.1 V *vs* RHE) after treatment with n-butyllithium suggesting the introduction of new active sites. Finally, a potential use in Lithium ion batteries (LIB) was examined. Our material can be used directly without any binder, additive carbon or copper current collector and delivers specific capacity of 740 mA h g^{-1} at a current density of 0.1 A g^{-1}. After 40 cycles at this current density the material still reached a capacity retention of 91%. Our findings show that this composite material could find application in electrochemical energy storage and generation devices where high flexibility and mechanical strength are desired.

Keywords

Flexible composites, batteries, supercapactors, hydrogen evolution, molybdenum disulfide

Introduction

The growing world's population has a nearly ever-and-ever increasing demand for energy. Due to the well-known problem of global warming, there are efforts to shift the energy production from burning fossil fuels towards renewable energy sources. But most of the renewable energy sources are not suitable for meeting the baseload requirements. Hence, energy storage and conversion is an important issue.[1, 2] Lithium ion batteries (LIBs) belong to the most excellent energy storage devices combining a high energy density and extremely low self-discharge. Nevertheless, in order to fulfill the (prospective) requirements to extend their application in large

energy storage systems or in the electromobility-sector, an improvement for example of the energy storage capacity is necessary. Layered dichalcogenide materials like molybdenum sulfide (MoS_2) are promising candidates in replacing the commercial anode material graphite. During charge/discharge, MoS_2 undergoes a 4-electron process resulting in theoretical specific capacity of 669 mAh g^{-1} which is almost two times higher than that of graphite (372 mAh g^{-1}).[3] However, the poor electrical conductivity, capacity fading and large volume changes upon charge and discharge make the commercialization of MoS_2 in LIBs still challenging.[3, 4] In order to address this issue, fabricating composites of MoS_2 and carbonaceous support materials such as amorphous carbon[5], carbon nanofibers[4], carbon nanotubes[5] and graphene[6] was already demonstrated to be quite attractive. Typically, the electrodes are prepared by mixing those composites as active material with a polymeric binder, conductive carbon and usually organic solvent to form a slurry, which is then coated onto a copper foil (current collector). The copper foil and the additives lead to extra weight which decreases the gravimetric energy density dramatically. Additionally, those electrodes are not applicable as anodes in flexible batteries due to the loss of contact between the active material and the current collector upon bending deformation.[7] But there are promising reports on freestanding MoS_2/carbonaceous composite electrodes which demonstrated an attractive electrochemical performance.[6-8, 9-13]

Beside LIBs, supercapacitors (SC) are seen as next generation energy storage devices having a high specific power, fast charge-discharge rates and excellent cycling stability.[2] Free-standing, binder free electrodes are also of great interest, as they can be used in flexible SCs.[14] In this regard, two-dimensional (2D) graphene attained lots of interest. Nevertheless, materials with higher performance are necessary.[14, 15] MoS_2 is seen, due its layered, graphene analogous structure as a

promising alternative providing a large surface area, which is favorable for double layer charge storage.[15, 16] Moreover, Mo can occupy multiple oxidation states which enables a pseudo-capacitive charge transfer by insertion of electrolyte ions, like Li^+, Na^+, K^+ and H^+.[16, 17] But upon cycling, the MoS_2 sheets can restack resulting in a decreased surface area, which is then followed by a poor capacitive performance. Introducing support materials, like graphene or carbon nanotubes (CNT) can alleviate this problem and improve the performance of the material.[14] Another popular related field in the context of energy storage and sustainable energy production is water splitting in order to produce hydrogen. The best catalysts for the hydrogen evolution reaction (HER) are unequivocally based on platinum and iridium but the scarcity and the high costs are tremendous disadvantages for the production of hydrogen in an industrial dimension.[9] Hence, it's necessary to develop new catalysts which are abundant, cheap and chemically robust.[9] MoS_2 is again a promising candidate. Theoretical and experimental studies successfully demonstrated that nanosized MoS_2 is more applicable than the bulk phase. The surface of the bulk phase mainly consists of thermodynamically more stable basal sites, which are catalytically less active. In contrast, sulfur edge sites of MoS_2 are highly catalytically active towards HER.[18] However, MoS_2 possesses only a low intrinsic conductivity which hinders the charge transport.[19] Using MoS_2 together with conducting support materials, like multi-walled carbon nanotubes (MWCNT) demonstrated improved catalytic properties.[19]

Herein, we report the synthesis of a freestanding MoS_2 based composite paper using small addition of single-walled carbon nanotubes (SWCNT) and shear force milling in *N*-Methyl-2-pyrrolidone (NMP). The paper was prepared simply by vacuum filtration of the slurry on top of a filter. The resulting material exhibits high flexibility and combines high conductivity of SWCNTs and electrochemical potential of MoS_2. We

show that the material finds use as anodes in LIBs, supercapacitor electrodes and HER catalyst. Use in LIBs seems particularly promising as this composite material requires no additional binders, conductive additives or a current collector.

Results and Discussion

Characterization of morphology, composition and mechanical properties

The synthesized composite material based on MoS_2 and SWCNTs was prepared by shear force milling of MoS_2 powder with SWCNTs. We then prepared a paper-like material by filtration of the mixture on top of a filter. The self-assembled material was denoted as MoS_2 based composite paper. An image of such a MoS_2 based composite paper is shown in Figure 1.

Figure 1. Image of the MoS_2 based composite paper showing its size and flexibility.

We investigated the morphology of this compound material by scanning electron microscopy (SEM) with results shown in **Figure 2**. The morphology images of the top side of the composite paper (**Figure 2a and 2b)** show homogeneous distribution of SWCNTs among the MoS_2 sheets. SEM micrographs of the cross-section (**Figure 2c**

and 2d) also illustrate that the SWCNTs significantly contribute to the flexibility and mechanical strength of the composite as they hold individual sheets together. We also performed the characterization of composition by energy dispersive spectroscopy (EDS). The elemental composition maps (**Figure S1**) have revealed a homogeneous distribution of elements. We have also identified (**Table S1**) that there was about 2.1wt. % of iron in the sample. This contamination originates from the carbon nanotubes, where iron usually serves as a catalyst for their growth.[20]
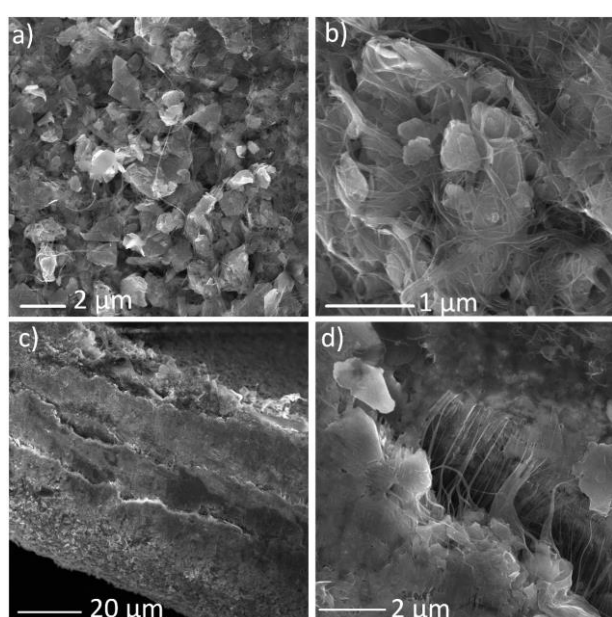

Figure 2. SEM micrographs of a) and b) plane and its c) and d) cross-section at different magnifications.

X-ray photoelectron spectroscopy (XPS) was used to track the degree of degradation of the MoS_2 sheets. Components originating from MoS_2 and MoO_3 were identified in the core-level Mo 3d spectrum (**Figure 3**). The positions of the individualcomponents are in agreement with previous reports for MoS_2 and MoO_3.[21] The deconvolution revealed that the MoO_3 content was about ~ 12at.%. This degree of oxidation is lower than in the case of chemically exfoliated MoS_2, possibly due to slightly lower

degree of exfoliation.[22] Additionally, no oxidation was observed for sulfur as only states originating from sulfides were identified in the S 2p spectrum (**Figure 3b**).[23]
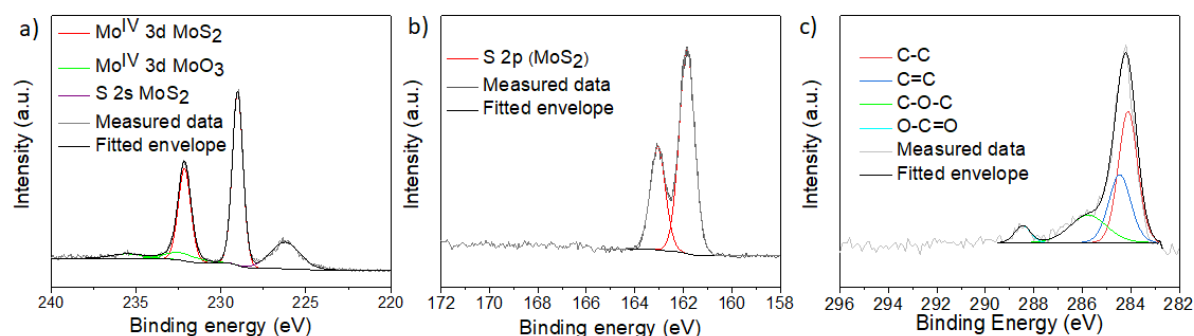

Figure 3. Core-level X-ray photoelectron spectra of a) Mo 3d region, b) S 2p region, c) C 1s region.

Chemical states for the SWCNTs could not be determined precisely due to the overlap with adventitious carbon. However, the conditions used during our experiment were highly unlikely to cause any chemical changes in the SWCNTs. Additionally, mechanical properties of prepared MoS_2 based composite paper were evaluated. Tensile strength and tensile ductility are important material parameters that influence material´s final applicability. The tensile strength of the prepared material reached a value of 3.02 MPa while tensile ductility was 7.74%. It should be mentioned that preparation of paper solely from MoS_2 sheets is not possible since there is no material holding individual MoS_2 sheets together. On the other hand, paper made of only SWCNT possesses tensile strength of 5.95 MPa and tensile ductility of 2.45%. Thus, incorporation of MoS_2 sheets into SWCNT paper results in decreased tensile strength and increased tensile ductility and the as-prepared MoS_2 based composite paper is able to undergo significant plastic deformation before rupture in the material occurs. Results of mechanical properties are summarized in **Table 1**.

Table 1. Tensile strength and ductility of MoS$_2$ based composite paper and pure SWCNT-paper.

Sample	Tensile strength (MPa)	Tensile ductility (%)
MoS$_2$ based composite paper	3.02	5.95
Pure SWCNT paper	7.74	2.45

Electrochemical performance of freestanding MoS$_2$ based composite paper

First, we tested the MoS$_2$ based composite paper for applications in supercapacitors (SC). Capacitance was measured by chronoamperometry technique in KCl solution (1 M) using different charging-discharging current densities (1-5 mA cm^{-2}) in a potential range determined by cyclic voltammetry (CV) shown in **Figure S2**. CV curves demonstrate the rectangular shape pointing out to the electric double layer capacitance as the origin of capacitive behavior. Capacitance C in mF cm^{-2} was calculated from the value of discharging current I, discharging time t, maximal voltage U and area of electrode that comes to contact with electrolyte solution S. Calculation was performed using equation:

$$C = \frac{2.I}{S.\frac{U}{t}}$$

Calculated values are summarized for each discharging current in **Table 2**. Charging-discharging curves of MoS$_2$ based composite paper obtained using chronoamperometry measurement are shown in **Figure 4**. We also compared capacitance of our composite MoS$_2$ based composite paper with other reported

materials (see **Table 3**). Capacitance of our composite material exhibits competitive value compared to other materials reported in literature.

Table 2. Capacitance of MoS_2 based composite paper measured using various discharging current densities.

MoS$_2$ based composite paper						
Discharging current density (mA.cm^{-2})	1	2	3	4	5	6
Capacitance (mF.cm^{-2})	70	40	35	33	29	28

Table 3. Performance of various electrode materials

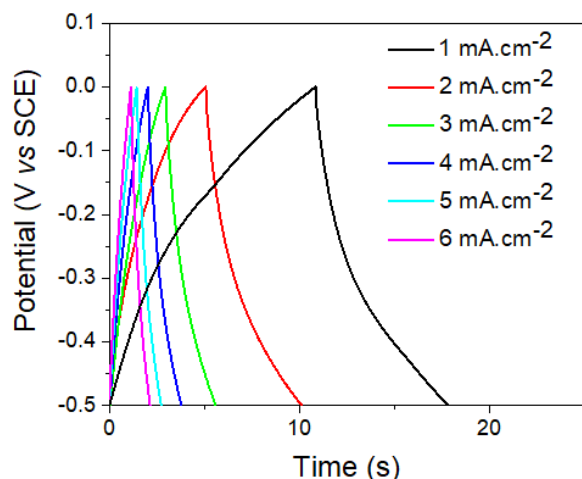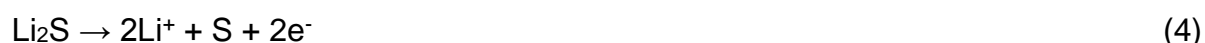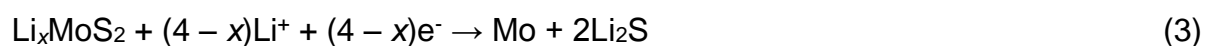| Reference	Electrode material	Electrolyte	Capacitance (mF cm^{-2})
This work	MoS$_2$ based composite paper	KCl	33
[34]	interdigital MWCNT electrode	PVA-KOH	107.3
[35]	CNT	PVDF-HFP/EMIMTFSI	2.88
[36]	graphene	PVA-H$_2$SO$_4$	2.32
[37]	Graphene-CNT	KCl	2.8

Figure 4. Charging-discharging curves of MoS₂ based composite paper obtained by chronoamperometry in 1M KCl solution using different current densities.

The freestanding MoS₂ based composite paper was also tested as anode material for LIBs. Hence, the MoS₂ based composite paper was directly used as anode without any binder, carbon additive or a Cu-foil current collector. **Figure 5a** shows the first four cycles of cyclic voltammetry (CV) curves of the MoS₂ based composite paper. The measurements were performed at a scan rate of 0.1 mV s⁻¹ in the voltage range of 0.01-3.0 V *vs* Li/Li⁺. In the initial cathodic scan, two dominant reduction peaks at around 1.0 and 0.3 V are detectable (**Figure 5a**). The first can be associated with the insertion of lithium ions into the van der Waals spaces between the MoS₂ layers forming LiₓMoS₂ accompanied by a phase transformation from trigonal prismatic (2H) to octahedral (1T) (reaction (2)).[5, 12, 13] The peak at ~0.3 V corresponds to the conversion of the previously formed LiₓMoS₂ into metallic Mo and LiS₂ (reaction (3)) and the decomposition of the electrolyte followed by the formation of a solid electrolyte interphase (SEI) layer.[11, 12] The prominent anodic peak at ~2.5 V results from the conversion of Li₂S to sulfur and lithium ions (reaction (4)).[12] During the following discharge cycles the two peaks at ~1.0 and ~0.3 V diminish and three

10

new reduction peaks at around 1.8, 1.1 and 0.3 V appear which can be ascribed to the following reactions (Eq. 1-3):

$$2Li^+ + S + 2e^- \rightarrow Li_2S \qquad (1)$$

$$MoS_2 + xLi^+ + xe^- \rightarrow Li_xMoS_2 \qquad (2)$$

$$Li_xMoS_2 + (4 - x)Li^+ + (4 - x)e^- \rightarrow Mo + 2Li_2S \qquad (3)$$

$$Li_2S \rightarrow 2Li^+ + S + 2e^- \qquad (4)$$

Hence, the reduction peak at ~1.8 V and the oxidation peak at 2.5 V form together a reversible redox couple.[12] Starting with the second cycle, a shallow oxidation peak arises at ~1.7 V which can be attributed to the partial oxidation of metallic Mo to MoS_2.[13, 24]

Moreover, the electrochemical performance of the MoS_2 based composite paper is evaluated by galvanostatic discharge/charge measurements, as well. The lithiation and delithiation plateaus (**Figure 5b**) obtained at a current density of 0.2 A g^{-1} are in consistent with the reduction and oxidation peaks gathered from the CV measurement.
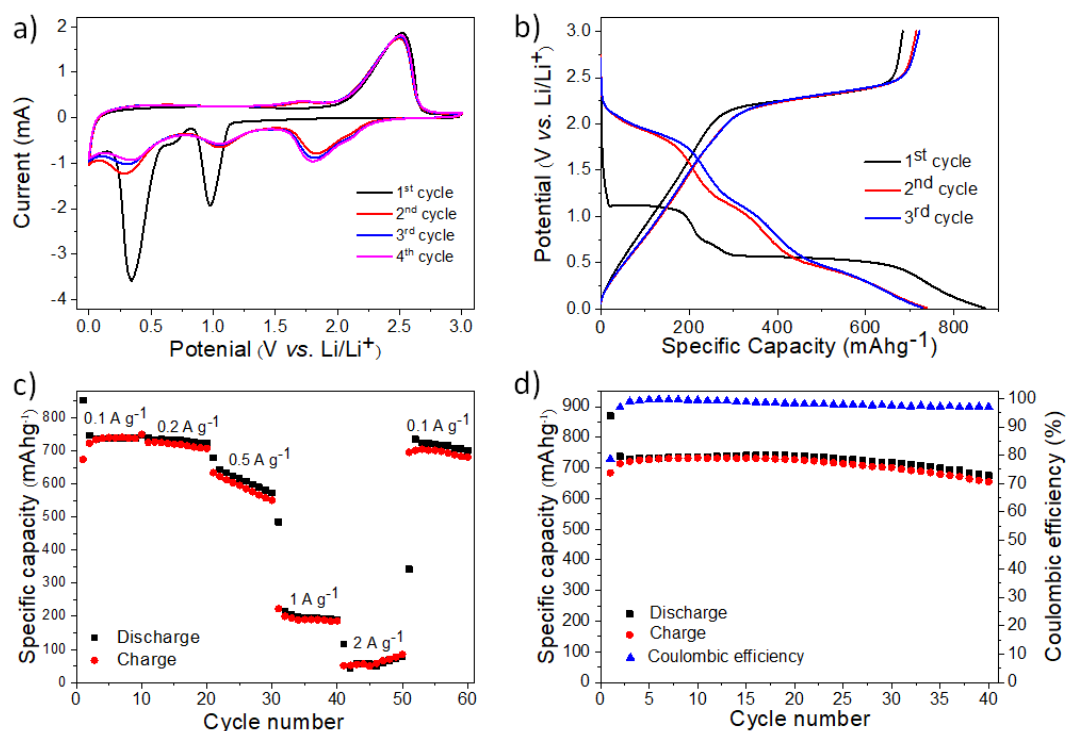
Figure 5: Electrochemical analysis of the freestanding MoS$_2$ based composite paper. (a) CV curves at a scan rate of 0.1 V s^{-1}, (b) discharge/charge voltage profiles at 0.2 A g^{-1}, (c) reversible capacities at different current densities ranging from 0.1 to 2.0 A g^{-1} and (d) cycling performance and Coulombic efficiency at 0.2 A g^{-1}.

In the first cycle, discharge and charge capacities of 870 and 684 mA h g^{-1} are obtained, respectively which correspond to a Coulombic efficiency of 79%, as shown in **Figure 5b** and **d**. The irreversible initial capacity loss is mainly attributed to the formation of the SEI layer.[5, 10, 12] During the subsequent cycles, Coulombic efficiencies of ≤97% are reached which implies a good cycling reversibility (**Figure 5d**). After 40 cycles a specific capacity of 675 mA h g^{-1} is reached equaling a capacity retention of 78% compared to the initial cycle or 91% when compared to the second cycle. It should be noted that for the calculation of the specific capacities the total mass of the freestanding MoS$_2$ based composite paper electrode was used.

12

Moreover, the rate performance of the freestanding MoS$_2$ based composite paper electrodes was further investigated (**Figure 5c**). The composite delivers 740, 721, 596, 190 and 49 mA h g^{-1}, at current rates of 0.1, 0.2, 0.5, 1 and 2 A g^{-1}, respectively. The slightly increasing capacity during the 2 A g^{-1} step may be attributed to high current rate activation of new Li$^+$ storage sites, originating from the opening up of blocked ends of SWCNTs.[5] Interestingly, when the current density was set back to 0.1 A g^{-1} the capacity reached 681 mA h g^{-1} (80th cycle) equaling to capacity retention of 91% compared to the second cycle, also confirming the high structural stability of the freestanding MoS$_2$ based composite paper. The kinetic analysis of the MoS$_2$ based composite paper is described in **Figure S2** and the SI.

Finally, we tested the MoS$_2$ based composite paper as a catalyst for hydrogen evolution reaction (HER). The results are shown in **Figure 6**. Apart from the pristine material, we also treated the paper with *n*-butyllithium (BuLi) solution to introduce new active sites in the form of edge sites as well as defects. Pristine as-prepared material exhibited an onset potential of about -0.195 V *vs* RHE. On the other hand, BuLi exfoliated MoS$_2$ based composite paper showed improved activity with an onset potential of about -0.095 V *vs* RHE. These differences clearly demonstrate that new sites were indeed introduced by the treatment. However, **Figure 6** also demonstrates that BuLi treated samples exhibited substantially higher (171 mV/dec) Tafel slope value than the pristine sample (105 mV/dec). This discrepancy could be caused by a loss of proper connection between MoS$_2$ sheets and SWCNTs and a decrease in conductivity. This claim is supplemented by the fact that the paper material exhibited lower flexibility than the original one.
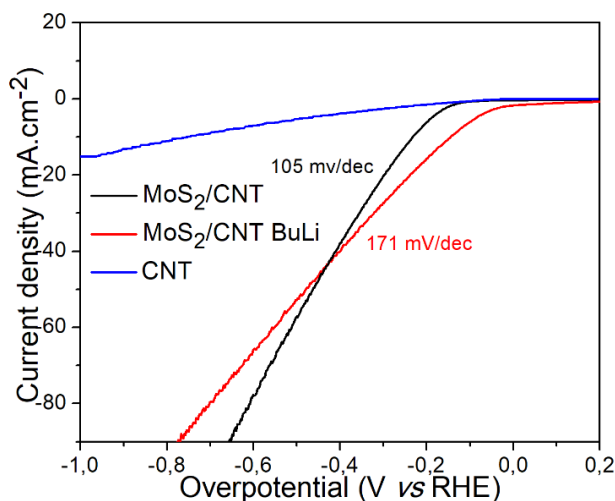
Figure 6. Linear sweep voltammetry curves for hydrogen evolution reaction measurements. 0.5 M H_2SO_4, 2 mV s^{-1}.

Conclusion

Using shear force milling, we have prepared free-standing MoS_2 based composite paper material. This method is very simple and takes advantage of the fact that a paper like material is self-assembled on top of a filter during vacuum filtration. The reported material exhibits high structural integrity and flexibility. The composite was tested in various electrochemical applications covering supercapacitors, anodes in lithium ion batteries and hydrogen evolution catalysis. In terms of supercapacitors, our material exhibits capacitance of 33 mF cm^{-2} at current density of 1 mA cm^{-2}. This value is competitive to other reported materials based on carbon nanomaterials. This material can also be used as a hydrogen evolution reaction catalyst. The as-prepared materials exhibits an onset potential of approximately -0.195 V *vs* RHE and is capable of reaching current densities as high as 100 mA cm^{-2}. Additionally, we treated the material with *n*-butyllithium to further enhance the HER activity. The resulting material exhibited lower onset potential, however, the exfoliation of MoS_2

14

sheets resulted in a loss of connection between the MoS_2 sheets and SWCNTs. Ultimately, this led to a decrease in conductivity and consequently, substantial increase in Tafel slope value. The MoS_2 based composite paper was also tested as a free-standing anode in LIBs without additives like binders or conductive agents. a. After the initial loss of specific capacity due to the formation of solid electrolyte interface, the composite delivers specific capacity of 740 mA h g^{-1} at 0.1 A g^{-1}. Moreover, the material retains 91% of its capacity after 40 cycles. A high capacity retention was also observed after the rate performance tests. These findings show that the reported material is also promising for the application in (flexible) batteries.

Experimental

Materials

MoS_2 was purchased from Alfa Aesar, TUBALL SWCNTs were purchased from OCSiAl, *N*-Methyl-2-pyrrolidone (NMP) was purchased from Sigma Aldrich. PuriEL electrolyte (1.15 M $LiPF_6$ in ethylene carbonate/ethyl methyl carbonate/dimethyl carbonate (EC/EMC/DMC) = 2:2:6 v/v + 1.0 wt.% fluoroethylene carbonate (FEC), *soul*brain MI) and lithium metal (Rockwood) were used as received.

Preparation of MoS_2 based composite paper

125 mg of MoS_2 powder and 12.5 mg of SWCNTs were added to 80 mL of argon purged NMP. The suspension was then exfoliated under Ar atmosphere for 2 h at 16k rot/min. using high-energy shear-force disperser. After that, the mixture was vacuum filtered. The resulting paper like material was dried for several days under vacuum.

Battery Assembly and electrochemical measurements

The freestanding MoS_2 based composite paper were cut into round disks with a diameter of 18 mm (254.5 mm^2). They were directly used as anode in ECC-PAT-Core (EL-Cell) battery test cells assembled in an argon filled glove box using lithium metal both as counter and reference electrode and an EL-CELL ECC1-01-0011-A/L glass fiber membrane as separator. The used electrolyte consisted of a commercial mixture of 1.15 M $LiPF_6$ in EC/EMC/DMC at a 2:2:6 volume to volume ratio and 1.0 % wt FEC.

Electrochemical measurements were performed at room temperature using an Autolab potentiostat/galvanostat (PGSTAT302N) with a FRA32M module or an Autolab Multipotentiostat M101 with a 8AUT.M101 module operated with Nova 1.11 software. Cyclic voltammograms were recorded in a potential range of 0.01–3.0 V *vs* Li/Li^+ using scan rate ranging from 0.05 mV s^{-1} to 1 mV s^{-1}. The cells were charged and discharged galvanostatically at different C rates (0.1 to 2 A g^{-1}) in a voltage range of 0.01 – 3.0 V *vs* Li/Li^+.

Supercapacitors

Disk with diameter of 14 mm was cut-off from vacuum assembled MoS_2 based composite paper material. Then it was placed into electrochemical holder (InRedox, USA) which was placed in the middle of platinum basket (counter electrode). Saturated calomel reference electrode was used as reference electrode and measurements were performed in 1 M KCl solution. The exposed area was a disk with 0.94 mm diameter. In order to measure charge-discharge curves, several charging-discharging currents (1-5 mA cm^{-2}) were used to charge the material to -0.8 V *vs* SCE.

Hydrogen evolution reaction

For HER measurements, the pristine sample was placed in electrochemical holder (InRedox, USA) which was inserted into 0.5 M H_2SO_4 electrolyte with SCE and carbon rod as reference and counter electrodes, respectively. The scan rate was 2 mV s^{-1}. For n-butyllithium treated sample, the foil was left in n-butyllithium solution (2.5 M solution) for several days under inert Ar atmosphere. After that, water was added to the solution. The foil was then dried and used.

Characterizations

The morphology was investigated using scanning electron microscopy (SEM) with a FEG electron source (Tescan Lyra dual beam microscope). Elemental composition and mapping were performed using an energy dispersive spectroscopy (EDS) analyzer (X-MaxN) with a 20 mm^2 SDD detector (Oxford instruments) and AZtecEnergy software. 10 kV beam was used for the measurements.

High resolution X-ray photoelectron spectroscopy (XPS) was performed using an ESCAProbeP spectrometer (Omicron Nanotechnology Ltd, Germany) with a monochromatic aluminum X-ray radiation source (1486.7 eV). Wide-scan surveys of all elements were performed (0 – 1000 eV, step 0.5 eV) with subsequent high-resolution scans of the C 1s, S 2p and Mo 3d with step of 0.05 eV.

The dynamic mechanical analysis was measured on DMA DX04T (by RMI, Czech Republic). A sample with dimensions 7.600 mm (width), 0.173 mm (thickness) and 10.200 mm (active length) was loaded with a tensile longitudinal sinusoidal deformation with the amplitude of 0.02 mm and pre-tension of 0.03 mm. The temperature range was 20 to 200 °C with a heating rate of 2°C min^{-1} in the air

atmosphere. From the results, the values of moduli and loss factor were evaluated as the second order sliding average.
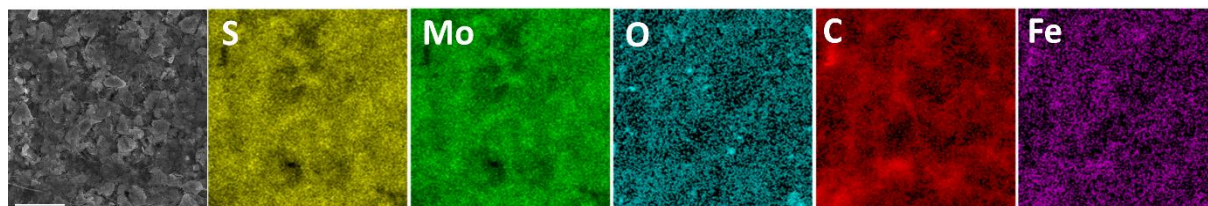
Supporting Information

Figure S1. Elemental distribution maps of the MoS$_2$/SWCNT-paper.

Table S1. Elemental composition obtained from SEM-EDS

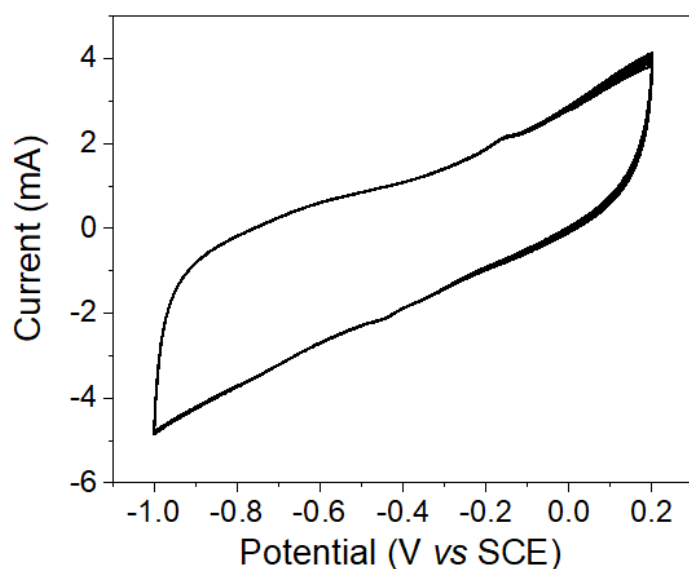| Sample	S wt.%	Mo wt.%	O wt.%	C wt.%	Fe wt.%
MoS$_2$ based composite paper	29.7	40.9	2.1	25.1	2.1

Figure S2. Cyclic voltammograms of MoS$_2$ based composite paper in 1 M KCl. Scan rate 100 mV s^{-1}.
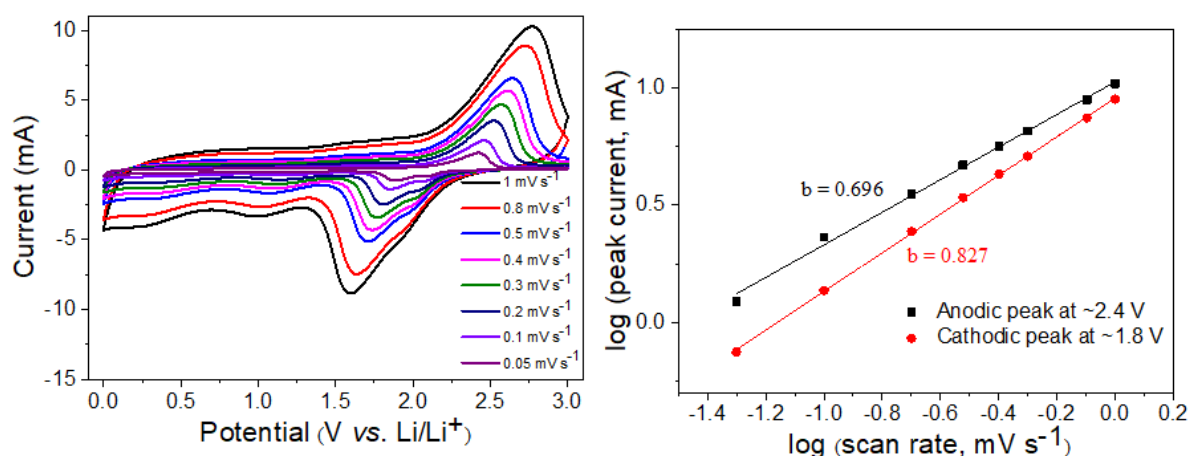
Kinetics analysis

Figure S3. Kinetic analysis of the freestanding MoS$_2$ based composite paper. (a) CV curves at different scan rates, (b) relationship between logarithmic peak current (cathodic peak at ~1.8 V and anodic peak at ~2.4 V) and logarithmic scan rates. CV measurements were conducted at different scan rates ranging from 1 to 0.05 mV s^{-1} to gain insights into the reaction kinetics (Figure S2). The degree of capacitive effect can be qualitatively analyzed according to the power law:

$$i = av^b \tag{5}$$

which relates the measured peak current (*i*) to the scan rate (*v*), *a* and *b* are adjustable parameters.[25] The *b* value can be determinate by fitting log(*i*) *versus* log(*v*) (FigureS2).[26] In general, *b* = 1 entails a capacitive surface-limited process, while *b* = 0.5 implies a semi-infinite linear diffusion-controlled mechanism.[25-27] For the cathodic peak at ~1.8 V and the anodic peak ~2.4 V *b* values of 0.827 and 0.696 were calculated, respectively. Those values indicate a higher capacitive contribution in the case of the reduction process compared to the oxidation analogue.

Acknowledgements

References

1. Hussain, A.; Arif, S. M.; Aslam, M. *Renewable and Sustainable Energy Reviews* **2017**, *71*, 12-28.
2. Sangeetha, D. N.; Selvakumar, M. *Applied Surface Science* **2018**, *453*, 132-140.
3. Liu, H.; Su, D.; Zhou, R.; Sun, B.; Wang, G.; Qiao, S. Z. *Advanced Energy Materials* **2012**, *2* (8), 970-975.
4. Zhou, F.; Xin, S.; Liang, H.-W.; Song, L.-T.; Yu, S.-H. *Angewandte Chemie International Edition* **2014**, *53* (43), 11552-11556.
5. Zhang, Z.; Zhao, H.; Teng, Y.; Chang, X.; Xia, Q.; Li, Z.; Fang, J.; Du, Z.; Świerczek, K. *Advanced Energy Materials* **2017**, *8* (7), 1700174.
6. Chao, Y.; Jalili, R.; Ge, Y.; Wang, C.; Zheng, T.; Shu, K.; Wallace, G. G. *Advanced Functional Materials* **2017**, *27* (22), 1700234.
7. Ren, J.; Ren, R.-P.; Lv, Y.-K. *Chemical Engineering Journal* **2018**, *353*, 419-424.
8. Wang, T.; Sun, C.; Yang, M.; Zhao, G.; Wang, S.; Ma, F.; Zhang, L.; Shao, Y.; Wu, Y.; Huang, B.; Hao, X. *Journal of Alloys and Compounds* **2017**, *716*, 112-118; Kong, D.; He, H.; Song, Q.; Wang, B.; Lv, W.; Yang, Q.-H.; Zhi, L. *Energy & Environmental Science* **2014**, *7* (10), 3320-3325, 10.1039/C4EE02211D; Rana, K.; Singh, J.; Lee, J.-T.; Park, J. H.; Ahn, J.-H. *ACS Applied Materials & Interfaces* **2014**, *6* (14), 11158-11166; Xie, D.; Tang, W. J.; Xia, X. H.; Wang, D. H.; Zhou, D.; Shi, F.; Wang, X. L.; Gu, C. D.; Tu, J. P. *Journal of Power Sources* **2015**, *296*, 392-399; Wang, Y.; Ma, Z.; Chen, Y.; Zou, M.; Yousaf, M.; Yang, Y.; Yang, L.; Cao, A.; Han, R. P. S. *Advanced Materials* **2016**, *28* (46), 10175-10181; Wang, B.; Guo, R.; Zheng, M.; Liu, Z.; Li, F.; Meng, L.; Li, T.; Luo, Y.; Jiang, H. *Electrochimica Acta* **2018**, *260*, 1-10; Deng, Z.; Jiang, H.; Hu, Y.; Liu, Y.; Zhang, L.; Liu, H.; Li, C. *Advanced Materials* **2017**, *29* (10), 1603020; Deng, Y.; Ding, L.; Liu, Q.; Zhan, L.; Wang, Y.; Yang, S. *Applied Surface Science* **2018**, *437*, 384-389.
9. Zhang, Q.; Xu, Z.; Lu, B. *Energy Storage Materials* **2016**, *4*, 84-91.
10. Malinský, P.; Cutroneo, M.; Macková, A.; Hnatowicz, V.; Szökölová, K.; Bohačová, M.; Luxa, J.; Sofer, Z. *Surface and Interface Analysis* **2018**, *50* (11), 1110-1115, Conference Paper.
11. *AIP Conference Proceedings*, 2018 https://www.scopus.com/inward/record.uri?eid=2-s2.0-85054178862&doi=10.1063%2f1.5053388&partnerID=40&md5=7c5c17feee510118f38de4df51e639f5.

12. Zhao, H.; Wu, J.; Li, J.; Wu, H.; Zhang, Y.; Liu, H. *Applied Surface Science* **2018**, *462*, 337-343.
13. Wang, W.; Yang, P.; Jian, Z.; Li, H.; Xing, Y.; Zhang, S. *Journal of Materials Chemistry A* **2018**, *6* (28), 13797-13805, 10.1039/C8TA03272F.
14. Ge, Y.; Jalili, R.; Wang, C.; Zheng, T.; Chao, Y.; Wallace, G. G. *Electrochimica Acta* **2017**, *235*, 348-355.
15. Lamberti, A. *Materials Science in Semiconductor Processing* **2018**, *73*, 106-110.
16. Choudhary, N.; Patel, M.; Ho, Y.-H.; Dahotre, N. B.; Lee, W.; Hwang, J. Y.; Choi, W. *Journal of Materials Chemistry A* **2015**, *3* (47), 24049-24054, 10.1039/C5TA08095A.
17. Acerce, M.; Voiry, D.; Chhowalla, M. *Nature Nanotechnology* **2015**, *10*, 313.
18. Kamila, S.; Mohanty, B.; Samantara, A. K.; Guha, P.; Ghosh, A.; Jena, B.; Satyam, P. V.; Mishra, B. K.; Jena, B. K. *Scientific Reports* **2017**, *7* (1), 8378; Benck, J. D.; Hellstern, T. R.; Kibsgaard, J.; Chakthranont, P.; Jaramillo, T. F. *ACS Catalysis* **2014**, *4* (11), 3957-3971; Zhang, G.; Liu, H.; Qu, J.; Li, J. *Energy & Environmental Science* **2016**, *9* (4), 1190-1209, 10.1039/C5EE03761A.
19. Cao, J.; Zhou, J.; Zhang, Y.; Liu, X. *Scientific Reports* **2017**, *7* (1), 8825.
20. Homma, Y.; Kobayashi, Y.; Ogino, T.; Takagi, D.; Ito, R.; Jung, Y. J.; Ajayan, P. M. *The Journal of Physical Chemistry B* **2003**, *107* (44), 12161-12164.
21. Brown, N. M. D.; Cui, N.; McKinley, A. *Appl. Surf. Sci.* **1998**, *134* (1), 11-21; Spevack, P. A.; McIntyre, N. S. *The Journal of Physical Chemistry* **1992**, *96* (22), 9029-9035.
22. Luxa, J.; Vosecký, P.; Mazánek, V.; Sedmidubský, D.; Pumera, M.; Sofer, Z. *ACS Catalysis* **2018**, *8* (4), 2774-2781.
23. Ganta, D.; Sinha, S.; Haasch, R. T. *Surface Science Spectra* **2014**, *21* (1), 19-27.
24. Wu, M.; Xia, S.; Ding, J.; Zhao, B.; Jiao, Y.; Du, A.; Zhang, H. *ChemElectroChem* **2018**, *5* (16), 2263-2270.
25. Xia, S.; Wang, Y.; Liu, Y.; Wu, C.; Wu, M.; Zhang, H. *Chemical Engineering Journal* **2018**, *332*, 431-439.
26. Wu, J.; Lu, Z.; Li, K.; Cui, J.; Yao, S.; Ihsan-ul Haq, M.; Li, B.; Yang, Q.-H.; Kang, F.; Ciucci, F.; Kim, J.-K. *Journal of Materials Chemistry A* **2018**, *6* (14), 5668-5677, 10.1039/C7TA11119C.
27. Wang, G.; Zhang, J.; Yang, S.; Wang, F.; Zhuang, X.; Müllen, K.; Feng, X. *Advanced Energy Materials* **2017**, *8* (8), 1702254.